Analyzing Temporal Variations in Radon Concentrations: Identifying Trends and Changes

Mutlu Ichedef

mutlu.ichedef@ege.edu.tr

Ege Universitesi   https://orcid.org/0000-0002-8590-1187

İlayda Sapmaz

Ege University Institute of Nuclear Sciences: Ege Universitesi Nukleer Bilimler Enstitusu

Caner Taşköprü

Ege University Institute of Nuclear Sciences: Ege Universitesi Nukleer Bilimler Enstitusu

Research Article

Abstract

Radon is a well-known precursor for geodynamic events such as earthquakes and volcanic tremors. Radon concentration variations in soil gas have been monitored worldwide, and extreme radon values have been identified as radon anomalies associated with geodynamic events. A radon time series contains many noise signals, primarily based on meteorological effects. Therefore, detecting anomalies from values outside the mean plus a few standard deviations or from values outside the average distribution threshold may not always yield good results. Instead of analyzing specific radon anomalies, an alternative method can be used to analyze the trend changes in the radon time series. This study examines locally estimated scatterplot smoothing (LOESS) to identify changes in the trend of the radon time series. During the two-year period of measurements, two separate groups with radon concentration anomalies and anomaly mechanisms were identified. In the first group, radon increases before the earthquake and decreases after the earthquake, while in the second group it shows the opposite behavior.

Introduction

Earthquake prediction remains one of the most challenging and essential problems faced by scientific communities. For earthquake prediction, potential precursors such as ^{222}Rn, CO_2, He, Cl^-, SO_4^{2-} and stable isotope ratios (δ^2H and $\delta^{18}O$) have been monitored in several fault zones, volcanoes and glaciers for the past few decades (Igarashi et al. 1995; Yang et al. 2005; Neri et al. 2006; Cicerone et al. 2009; Giammanco et al. 2010; Richon et al. 2012; Skelton et al. 2014; Yuce et al. 2017; Terray et al. 2020). Radon, one of the most widely used precursors, has been widely examined due to its relatively short half-life, being a noble gas and being continuously produced by the decay of uranium in the earth's crust. As an inert gas, it has no chemical compounds and its diffusive and advective behavior allows it and other gases to move easily. On the other hand, radon is produced in the uranium decay series, which is one of the most important reasons why it is a unique precursor. Many studies have shown that radon gas concentrations vary widely around fault lines/zones and can provide some signals for an earthquake (Papastefanou et al. 2001; Planinić et al. 2004; Walia et al. 2005, 2013; Giammanco et al. 2007; Içhedef et al. 2014; Tarakçi et al. 2014; Fu et al. 2019; İçhedef et al. 2020; Dhar et al. 2021; Masruoğlu et al. 2023; Muhammad et al. 2023). In these studies, the time-dependent change in radon concentration was analyzed, and earthquake-related radon anomalies were identified in the radon time series. A radon time series mostly contains many noise signals that need to be eliminated. To overcome this difficulty, researchers have focused on defining radon anomalies by different approaches. The most commonly used method is the mean ± nσ method (n = 1, 2, 3…), where values outside the standard deviation are considered anomalies (Virk and Walia 2001; Zmazek et al. 2002; Zhang et al. 2022). A secondary method is based on nonparametric tests in which a threshold of deviation from a normal distribution is determined in QQ plot curves and values exceeding this threshold are considered anomalies (Kafadar and Spiegelman 1986; Cheng et al. 1994; Yuce et al. 2017). The selection of earthquakes for analysis is another aspect that requires careful consideration. Some researchers consider earthquakes within a 20, 30, or 40 km radius around the corresponding measurement point (Sac et al. 2011), while others eliminate

earthquakes using the distance equation proposed by (Dobrovolsky et al. 1979). Alternatively, some researchers only consider earthquakes that occur in fault zones and at radon measurement locations. These choices will have significant impacts on the results.

Given the numerous options and choices involved, there is a need to conduct preliminary studies that examine radon concentrations in the region, determine radon averages, trends and analyze changes before establishing the relationship between radon and earthquakes. This approach will help ensure a comprehensive and reliable analysis of the data. To achieve that goal, the variation in soil gas radon levels in Bornova close to the Izmir Fault Zone (IF) was monitored for two years. This study aimed to determine the changes in soil gas radon concentrations by creating a primary dataset. We performed a time series analysis of the soil gas radon concentration to obtain baseline statistical data. Additionally, we investigated the characteristic pattern of long-term variations in soil gas radon concentrations rather than individual radon anomalies. We examined the LOESS to identify changes in the trend in radon concentrations.

Materials and Methods

Study area

Soil gas radon concentrations were measured in the backyard of the Institute of Nuclear Sciences, Ege University. The measurement point is close to the İzmir Fault Zone (IF) and Bornova Fault. The Izmir fault, which is a Quaternary fault, is located 3.3 km to the west. In the north, another fault, the Bornova fault, has a multiparty structure and a possible Quaternary fault or lineament (Fig. 1).

Tectonics of the study area

The continental collision between the Indian and Eurasia plates characterizes the seismo-tectonic activity of Turkey. The movement of these two plates is responsible for significant earthquakes in and around Anatolia. The Anatolian plate moves forward to the west under these forces at approximately 24 mm y^{-1} (McClusky et al. 2000). This movement turns counterclockwise in the west, turning into an expansion in the northeast-southwest direction. For this reason, a system was formed in which the western Anatolian horst-graben systems dominate, and the GPS shift rates are relatively lower (Uzel and Sözbilir 2008).

This study examined the change in soil gas radon concentrations in western Anatolia, which moves 2 cm westward each year and counterclockwise in the NE-SW direction because of the fragmented faulting of the Gediz Graben. During the study, a strong 6.6 magnitude earthquake occurred north of Samos Island (Greece) on October 30, 2020. This earthquake, which occurred approximately 70 km away from Izmir, caused significant damage in the city. The magnitude of the earthquake was Mw 6.9 according to (KOERI, 2023, Boğaziçi University Kandilli Observatory and Earthquake Research Institute), Mw 7.0 according to GFZ (GeoForschungs Zentrum, Helmholtz-Zentrum Postdam Deutsches), (AFAD, 2023, Disaster and Emergency Management Presidency Earthquake Department) According to OCA (GéoAzur, Université de Nice Sophia-Antipolis, Valbonne, France) Mw 7.2 (DAUM 2020). Nearly 3000 aftershocks with

magnitudes ranging from 1.0 to 5.3 were recorded from the main shock to 11.11.2020 (AFAD 2023; EMSC 2023). The main shock destroyed 17 buildings in the Bayraklı district (İzmir) in a short time and caused the deaths of 117 people. These devastating earthquakes confirmed the importance of our study and the importance of detecting radon variations before and after earthquakes.

Experimental Setup

Soil gas radon concentration data were collected for 2 years (2020–2021). Radon concentrations were measured using LR-115 Type 2 (Dosirad, France) solid-state nuclear track detectors to detect alpha particles emitted by radon and its decay products. An LR-115 Type 2 detector (1 cm x 1 cm) was attached to the bottom of the plastic cup. The cup was then covered with fiberglass filter paper. The plastic cup was placed in a deep hole inside the ground at a depth of approximately 100 cm (Vulkan et al. 1992; Papastefanou 2007). The sampling frequency was approximately three times a week (Monday, Wednesday, and Friday). At the end of the sampling period, the detector was replaced with a new one, and the old one was transferred to the laboratory for track etching. This process was carried out in an incubator containing 10% NaOH solution maintained at 60°C for 120 minutes, after which the detectors were incubated in distilled water for 20 minutes (İçhedef et al. 2013; Günay et al. 2018). Tracks on the detectors were counted under a digital microscope. Detailed information on the track etching and track counting processes is given in (Arias et al. 2005).

Earthquake Selection

Earthquake selection is a complex and challenging task due to the differences in distances between measurement point and earthquake locations. As mentioned above, different methodologies have been applied to overcome this problem. The earthquakes were selected by using the Dobrovolsky form: $R_D=10^{0.43M}$ (Dobrovolsky et al. 1979), where M is the magnitude of an earthquake, and R_D is an estimation of the radius of the zone within which precursor phenomena have been demonstrated. R_E is the distance between the earthquake epicenter and the measuring site. R_E values for earthquakes are taken as less than or equal to the R_D. The Dobrovolsky equation allows us to select earthquakes that can produce radon anomalies in the measurement location. The earthquake data (location, date, magnitude, depth, etc.) were obtained from AFAD, (2023). Throughout the study period, a total of 15 earthquakes were selected, and both radon and earthquake data were interpreted based on this assumption. (Table 1).

Table 1. The selected earthquakes around the study area (the consecutive earthquakes are highlighted in the same color, AFAD, 2023)

Earthquake no	Date	Longitude	Latitude	Magnitude	Distance (km)	Location
1	04.02.2020	27.8668°	38.9893°	4.8	81.6	Akhisar (Manisa)
2	18.02.2020	27.8453°	39.1015°	5.2	89.9	Kırkağaç (Manisa)
3	24.02.2020	27.8676°	38.9796°	4.8	80.9	Akhisar (Manisa)
4	09.06.2020	27.2208°	38.2515°	3.8	22.8	Menderes (İzmir)
5	26.06.2020	27.8018°	38.7676°	5.5	61.3	Saruhanlı (Manisa)
6	03.07.2020	27.5290°	38.5235°	3.7	27.9	Şehzadeler (Manisa)
7	30.10.2020	26.7995°	37.8406°	4.7	77.7	Aegean Sea-Seferihisar (İzmir)
8	30.10.2020	26.8216°	37.8520°	4.8	75.7	Aegean Sea-Seferihisar (İzmir)
9	30.10.2020	26.8690°	37.8331°	5.1	75.8	Aegean Sea-Seferihisar (İzmir)
10	30.10.2020	26.7030°	37.8790°	6.6	78.5	Aegean Sea-Seferihisar (İzmir)
11	31.10.2020	26.8303⁰	37.8701°	5.0	73.5	Aegean Sea-Seferihisar (İzmir)
12	01.02.2021	26.0788°	38.9483°	5.1	113.4	Aegean Sea-Seferihisar (İzmir)
13	01.02.2021	26.1185°	38.9850°	5.1	112.4	Aegean Sea-Seferihisar (İzmir)
14	19.05.2021	27.0090°	38.0826°	4.2	45.5	Menderes (İzmir)
15	19.05.2021	27.0295°	38.0876°	4.3	44.3	Menderes (İzmir)

Results and Discussion

Descriptive Statistics

Soil gas radon concentrations were determined between 2020 and 2021 at the Institute of Nuclear Sciences' backyard. The soil gas radon concentrations varied from 2178.6 to 22706.3 with a mean value of 10655 Bq m^{-3}. As reported by many authors (Ciotoli et al. 2014; Zafrir et al. 2016), global soil gas radon concentrations are in the range of kBq m^{-3}, and our results are consistent with the literature. In a previous study (İçhedef et al. 2013), soil gas radon concentrations were determined between 0.1 and 261.1 Bq m^{-3} around the Tuzla fault, which passing through the west of Izmir city center. The radon levels of this study are relatively low and vary within a narrow range. In another work, soil gas radon concentrations measured around the Manisa Fault varied between 0.2 and 35.2 kBq m^{-3}, and the average radon concentration was 4.84 kBq m^{-3} (Taşköprü et al. 2023). This fault passes northeast of the İzmir city center and is approximately 30 km from our measurement location. Descriptive statistics for the radon data are given in Table 2. The mean and median values are very close, while the mod has three values: 676.2, 7888.0, and 12620.9. Kurtosis is calculated as 0.5159 in the range between − 3 and + 3, and skewness is 0.4465, which should be close to zero, indicating that the radon data fit a normal (Gaussian) distribution.

Additionally, the Kolmogorov-Smirnov test was applied to check normality, and there was no significant deviation from the normal distribution (p = 0.75). As a result, the radon time series has some outliers, but these extreme values do not destroy normality. The descriptive statistical analysis was conducted in R and Rstudio (RStudio Team 2019; Team R C 2020), and figures were prepared with the package ggplot2 (Wickham et al. 2019).

Table 2
Descriptive statistics for radon

	Radon (Bq m^{-3})
Min	2178.6
Max	22706.3
Median	10442.3
Mean	10655.4
Mod	7888.0
	12620.9
	6761.2
Standard Dev.	3585.5
Skewness	0.52
Kurtosis	0.45
Test of Normality	0.75

Boxplots, histograms, Q-Q plots, and ECDF plots of ^{222}Rn activity in Fig. 2 show the detailed analysis of the radon data distribution.

Radon Time Series

A time series was obtained from two-year soil gas radon data, as shown in Fig. 3. It seems clear that the raw radon data (black line in Fig. 3) varied over a more comprehensive range during the study period, and large variations were observed, caused mainly by sharp and marked decreases in the measured radon activities. It is not easy to evaluate raw radon data regarding seismicity without a connected scatterplot containing many peaks. Therefore, it is difficult to determine the dominant trend. To obtain the best-fit trend, we added a smooth curve and its uncertainty in the form of point-wise confidence intervals, shown in grey. Locally estimated scatterplot smoothing, or LOESS, a nonparametric method for smoothing a series of data in which no assumptions are made about the underlying structure of the data, was applied to the raw data. LOESS uses local regression to fit a smooth curve through a connected scatterplot, and

this approach is effective when there are outliers in the dataset. The LOESS methodology includes techniques for constructing confidence intervals around the curve.

The trend line (Blue line) and confidence intervals (shown in yellow) in Fig. 3 give a clearer idea of the trend of radon. In a further analysis, we graphed a chart containing the radon trend and earthquakes and tried to interpret this graph (Fig. 4).

At the beginning of the study, three earthquakes, ranging in magnitude from 4.8 to 5.2, occurred near Manisa. The epicenters of these earthquakes were approximately 50 km northeast of our measurement location. The radon concentration shows an increasing trend with a minimal slope in this period (during the first 30 measurements) and then a slight decrease followed by a sharper increase between the 30th and 50th measurements. It is noteworthy that no earthquakes occurred for approximately 4-month period between the 10th and 50th measurements. The increased trend was over after three earthquakes occurred in 25 days (50th to 60th measurements). The radon behavior changed after these earthquakes, and a decreasing trend was observed for approximately 3 months from the beginning of July to the end of October. At the end of this period, the catastrophic Samos earthquake (M_L=6.6) and its aftershocks occurred. Nearly 3000 aftershocks were recorded in the first 11 days following the earthquake. Among these, only five earthquakes with magnitudes ranging from 4.7 to 6.6, capable of inducing radon anomalies, were selected. After the Samos earthquake, the radon trend line exhibited a relatively sharp increase. Compared to other earthquakes, it is observed that radon exhibited a marked decreasing trend following the Samos earthquakes, followed by a subsequent increase. A decrease was subsequently observed before the first earthquakes occurred in the Aegean Sea near Seferihisar in early February 2021.

A decrease was subsequently observed before the first earthquakes occurred in the Aegean Sea near Seferihisar in early February 2021. Then, the radon trend line continued to increase with a decreasing slope. This trend continued similarly until the two earthquakes in Menderes (Izmir) occurred on 19.05.2021. These earthquakes are the last earthquakes that occurred during the study period. The radon trend line gradually decreased during the period following these two earthquakes and followed a horizontal trend during the last 2 months of the study.

During the two-year period of measurements, two separate groups with radon concentration anomalies and anomaly mechanisms were identified. The first group is related to earthquakes numbered 4, 5, 6, 14, and 15, where radon concentration increased before these earthquakes and decreased afterward. The second group is associated with earthquakes numbered 7, 8, 9, 10, 11, 12, and 13, wherein radon concentration exhibited the opposite trend, increasing before these earthquakes and decreasing afterward. A comparable observation applies to earthquakes 1, 2, and 3; nonetheless, as these seismic events occurred at the outset of the investigation, no remarks can be made about radon alterations preceding them. Tarakçi et al. (2014) worked on stress-related pre-seismic soil gas radon variations in Tuzla fault another active fault near Izmir city. They reported that radon concentrations show significant differences in compression and expansion regions. Soil gas radon concentration levels increase before earthquakes and decrease towards the time of earthquake occurrence in a compression seismic area.

Conversely, radon levels do not show any changes before earthquakes and increase during earthquake occurrences in a dilation area. Their study area is a strike-slip fault with different characteristics compared to the İzmir Fault Zone (IF), which is a normal fault. In another study, results of the 26-year continuous observation data show different groups marked by significant large amplitude changes related to earthquakes. The first group data indicates that radon concentrations increased before the Xiuyan Mb 5.0 and MW 5.1 earthquakes and decreased afterward. The second group has the opposite behavior as the radon concentration increased sharply in the month following the earthquake. The last group shows a V-shaped progression before the earthquakes and initially low values after the earthquakes in 2013 (Zhou et al. 2020). Trend changes in radon may be related to fault characteristics and earthquake features such as depth, magnitude, distance, etc.

Radon is an inert gas that is not a chemical compound in nature. This feature makes it unique since its concentrations in soil gas are controlled by physical factors such as earthquakes, volcanic eruptions, and meteorological factors. Therefore, it is essential to consider meteorological factors such as atmospheric pressure, soil air temperature, relative humidity, rainfall, etc. These data were provided by the Turkish State Meteorological Service, which has a meteorological station approximately 1 km from the measurement station. The radon measurement dates were used to transform the meteorological data. Additionally, comparisons were made between the radon concentrations, average temperature, average pressure, and total precipitation data for consecutive years. This study, initiated in February 2020 and completed in February 2022, included a comprehensive review of these factors. Therefore, the first 12 months were compared with the results of the next 12 months. Remarkably, the soil gas radon concentrations exhibited comparable ranges in both years; the median values were close to each other. However, visualizing the data via a violin chart (Fig. 5) revealed distinct distribution differences. In the second year of the study, the radon concentrations ranged widely and had many more outliers than the first year. On the other hand, there were no significant changes in soil temperature or atmospheric pressure from year to year; significant differences were detected only in total precipitation. The total rainfall, which was 480 mm in the first year (2020), reached 824 mm in the second year (2021). This may also explain the differences in the distributions of radon concentrations among consecutive years.

The Pearson correlation coefficients between the soil gas radon concentration and meteorological parameters are shown in Fig. 6. Although the correlation coefficients are relatively low, the obtained results are consistent with the literature. First, there is a positive correlation between precipitation and relative humidity (r=-0.65). Similarly, there was an inverse correlation between soil temperature and relative humidity (r = 0.65). The soil temperature was positively correlated (r = 0.31) with the radon concentration. An inverse correlation (r=-0.11) was observed between radon and rainfall, similar to the findings of Ramola et al., 2008, where the correlation was r=-0,16. Briefly, a negative correlation was found between radon concentration and other parameters except temperature.

Conclusions

Soil gas radon anomalies have been identified in many studies using different methodologies, and some of them have proven that these anomalies are associated with an earthquake. However, the opposite results were obtained even in the same study. To eliminate this controversy, this study proposes analyzing the changes in the trend of radon instead of the trend in the anomalous radon concentration. The trend changes in radon time series analyzed with local earthquakes. This paper reports of two opposite precursory characteristics and mechanisms on a two-year temporal observation period. Each mechanism could be connected the fault characteristics and earthquake features such as depth, magnitude, distance, etc.

While the proposed method contributes only to the assessment of radon variation, how to select earthquakes around a measurement point is still unknown. This study presents an approach that can answer one of the many questions on the subject and seeks to change the point of view with a new proposal. New approaches are also needed for the selection of earthquakes and the evaluation of meteorological parameters.

Declarations

Ethics approval Not applicable.

Consent to Participate Not applicable.

Consent to Publish Not applicable.

Competing Interests Not applicable.

Data availability Data will be made available on a reasonable request.

References

1. AFAD (2023) AFAD,Disaster and Emergency Management Presidency Earthquake Department. https://deprem.afad.gov.tr/event-catalog

2. Arias H, Palacios D, Sajó-Bohus L, Viloria T (2005) Alternative procedure for LR 115 chemical etching and alpha tracks counting. Radiat Meas 40:357–362. https://doi.org/10.1016/j.radmeas.2005.05.020

3. Cheng Q, Agterberg FP, Ballantyne SB (1994) The separation of geochemical anomalies from background by fractal methods. J Geochem Explor 51:109–130. https://doi.org/10.1016/0375-6742(94)90013-2

4. Cicerone RD, Ebel JE, Britton J (2009) A systematic compilation of earthquake precursors. Tectonophysics 476:371–396. https://doi.org/10.1016/j.tecto.2009.06.008

5. Ciotoli G, Tartarello SB et al (2014) C, Journal of Geophysical Research : Solid Earth. AGU: Journal of Geophysical Research, Solid Earth 119:2440–2461. https://doi.org/10.1002/2013JB010508.Received

6. DAUM (2020) Dokuz Eylül Üniversitesi Deprem Araştırma ve Uygulama Merkezi. (DAUM)

7. Dhar S, Randhawa SS, Kumar A et al (2021) Decomposition of continuous soil–gas radon time series data observed at Dharamshala region of NW Himalayas, India for seismic studies. J Radioanal Nucl Chem 327:1019–1035. https://doi.org/10.1007/s10967-020-07575-x

8. Dobrovolsky IP, Zubkov SI, Miachkin VI (1979) Estimation of the size of earthquake preparation zones. Pure Appl Geophys PAGEOPH 117:1025–1044. https://doi.org/10.1007/BF00876083

9. EMSC (2023) EMSC,Euro-Méditerranéen, Centre Sismologique Euro Mediterranean Seismological Centre. https://emsc-csem.org/Earthquake_information/

10. Fu CC, Lee LC, Yang TF et al (2019) Gamma ray and Radon anomalies in Northern Taiwan as a possible preearthquake indicator around the plate boundary. https://doi.org/10.1155/2019/4734513. Geofluids 2019:

11. Giammanco S, Bellotti F, Groppelli G, Pinton A (2010) Statistical analysis reveals spatial and temporal anomalies of soil CO_2 efflux on Mount Etna volcano (Italy). J Volcanol Geoth Res 194:1–14. https://doi.org/10.1016/j.jvolgeores.2010.04.006

12. Giammanco S, Sims KWW, Neri M (2007) Measurements of ^{220}Rn and ^{222}Rn and CO_2 emissions in soil and fumarole gases on Mt. Etna volcano (Italy): Implications for gas transport and shallow ground fracture. Geochem Geophys Geosyst 8:1–14. https://doi.org/10.1029/2007GC001644

13. Günay O, Saç MM, İçhedef M, Taşköprü C (2018) Soil gas radon concentrations along the Ganos Fault (GF). Arab J Geosci 11:1–5. https://doi.org/10.1007/s12517-018-3542-2

14. İçhedef M, Giammanco S, Neri M et al (2020) In soil radon anomalies and volcanic activity on Mt. Etna (Italy). J Environ Radioact 218. https://doi.org/10.1016/j.jenvrad.2020.106267

15. İçhedef M, Saç MM, Camgöz B et al (2013) Soil gas radon concentrations measurements in terms of great soil groups. J Environ Radioact 126:165–171. https://doi.org/10.1016/j.jenvrad.2013.08.003

16. Içhedef M, Saç MM, Harmanşah C, Taskopru C (2014) Two year evolution of radon emission and tectonic movements in tuzla fault, seferihisar-İzmir. Appl Radiat Isot 86:102–108. https://doi.org/10.1016/j.apradiso.2013.12.011

17. Igarashi G, Saeki S, Takahata N et al (1995) Ground-water radon anomaly before the kobe earthquake in Japan. Science 269:60–61. https://doi.org/10.1126/science.269.5220.60

18. Kafadar K, Spiegelman CH (1986) An alternative to ordinary q-q plots: Conditional q-q plots. Comput Stat Data Anal 4:167–184

19. KOERI BUKO and ER (2023) KOERI. http://www.koeri.boun.edu.tr/scripts/lst1.asp

20. Masruoğlu G, Altun C, Şentürk MZ et al (2023) Variation of soil gas 222Rn/220Rn concentration ratios along the Pınarbaşı segment of İzmir fault. J Radioanal Nucl Chem 332:4739–4743. https://doi.org/10.1007/s10967-023-08910-8

21. McClusky S, Balassanian S, Barka A et al (2000) Global Positioning System constraints on plate kinematics and dynamics in the eastern Mediterranean and Caucasus. J Geophys Research: Solid Earth 105:5695–5719. https://doi.org/10.1029/1999jb900351

22. Muhammad A, Külahcı F, Birel S (2023) Investigating radon and TEC anomalies relative to earthquakes via AI models. J Atmos Solar Terr Phys 245:106037. https://doi.org/10.1016/j.jastp.2023.106037

23. Neri M, Behncke B, Burton M et al (2006) Continuous soil radon monitoring during the July 2006 Etna eruption. Geophys Res Lett 33:1–5. https://doi.org/10.1029/2006GL028394

24. Papastefanou C (2007) Measuring radon in soil gas and groundwaters: A review. Ann Geophys 50:569–578. https://doi.org/10.4401/ag-3070

25. Papastefanou C, Manolopoulou M, Stoulos S et al (2001) Radon measurements along active faults in the Langadas Basin, northern Greece. Nat Hazards Earth Syst Sci 1:159–164. https://doi.org/10.5194/nhess-1-159-2001

26. Planinić J, Radolić V, Vuković B, Accelerators A (2004) Spectrometers Detectors Assoc Equip 530:568–574. https://doi.org/10.1016/j.nima.2004.04.209

27. Ramola RC, Prasad Y, Prasad G et al (2008) Soil-gas radon as seismotectonic indicator in Garhwal Himalaya. Appl Radiat Isot 66:1523–1530. https://doi.org/10.1016/j.apradiso.2008.04.006

28. Richon P, Moreau L, Sabroux JC et al (2012) Evidence of both M 2 and O1 Earth tide waves in radon-222 air concentration measured in a subglacial laboratory. J Geophys Research: Solid Earth 117:1–9. https://doi.org/10.1029/2011JB009111

29. RStudio Team, RStudio (2019) RStudio: Integrated Development for R. Inc., Boston, MA. http://www.rstudio.com/

30. Sac MM, Harmansah C, Camgoz B, Sozbilir H (2011) Radon monitoring as the earthquake precursor in fault line in Western Turkey. Ekoloji 98:93–98. https://doi.org/10.5053/ekoloji.2011.7912

31. Skelton A, Andrén M, Kristmannsdóttir H et al (2014) Changes in groundwater chemistry before two consecutive earthquakes in Iceland. Nat Geosci 7:752–756. https://doi.org/10.1038/NGEO2250

32. Tarakçi M, Harmanşah C, Saç MM, Içhedef M (2014) Investigation of the relationships between seismic activities and radon level in Western Turkey. Appl Radiat Isot 83:12–17. https://doi.org/10.1016/j.apradiso.2013.10.008

33. Taşköprü C, Içhedef M, Oral AE et al (2023) The exchange of radon gas concentration along Manisa fault. J Radioanal Nucl Chem 332:4721–4737. https://doi.org/10.1007/s10967-023-08934-0

34. Team RC (2020) A language and environment for statistical computing. R Foundation for Statistical Computing, Vienna, Austria

35. Terray L, Gauthier PJ, Breton V et al (2020) Radon Activity in Volcanic Gases of Mt. Etna by Passive Dosimetry. J Geophys Research: Solid Earth 125:1–15. https://doi.org/10.1029/2019JB019149

36. Uzel B, Sözbilir H (2008) A first record of a strike-slip basin in Western Anatolia and its tectonic implication: The Cumaovasi basin. Turkish J Earth Sci 17:559–591

37. Virk HS, Walia V (2001) Helium/radon precursory signals of Chamoli Earthquake, India. Radiat Meas 34:379–384. https://doi.org/10.1016/S1350-4487(01)00190-1

38. Vulkan U, Steinitz G, Strull A, Zafrir H (1992) Long-distance (+ 100m) Transport of Radon in Syenitic Rocks at Makhtesh Ramon, Israel. Nucl Geophys 6:261–271

39. Walia V, Su TC, Fu CC, Yang TF (2005) Spatial variations of radon and helium concentrations in soil-gas across the Shan-Chiao fault, Northern Taiwan. Radiat Meas 40:513–516. https://doi.org/10.1016/j.radmeas.2005.04.011

40. Walia V, Yang TF, Lin SJ et al (2013) Temporal variation of soil gas compositions for earthquake surveillance in Taiwan. Radiat Meas 50:154–159. https://doi.org/10.1016/j.radmeas.2012.11.007

41. Wickham H, Averick M, Bryan J et al (2019) Welcome to the Tidyverse. J Open Source Softw 4:1686. https://doi.org/10.21105/joss.01686

42. Yang TF, Walia V, Chyi LL et al (2005) Anomalous radon emission as precursor of earthquake. J Appl Geophys 69:496–502. https://doi.org/10.1016/j.jappgeo.2009.06.001

43. Yuce G, Fu CC, D'Alessandro W et al (2017) Geochemical characteristics of soil radon and carbon dioxide within the Dead Sea Fault and Karasu Fault in the Amik Basin (Hatay), Turkey. Chem Geol 469:129–146. https://doi.org/10.1016/j.chemgeo.2017.01.003

44. Zafrir H, Horin YB, Uri M et al (2016) Journal of Geophysical Research : Solid Earth. AGU: Journal of Geophysical Research, Solid Earth 121:6346–6364. https://doi.org/10.1002/2016JB013033.Received

45. Zhang S, Shi Z, Wang G et al (2022) Application of the extreme gradient boosting method to quantitatively analyze the mechanism of radon anomalous change in Banglazhang hot spring before the Lijiang Mw 7.0 earthquake. J Hydrol 612:128249. https://doi.org/10.1016/j.jhydrol.2022.128249

46. Zhou Z, Tian L, Zhao J et al (2020) Stress-Related Pre-Seismic Water Radon Concentration Variations in the Panjin Observation Well, China (1994–2020). Front Earth Sci 8:1–12. https://doi.org/10.3389/feart.2020.596283

47. Zmazek B, Italiano F, Ivči M et al (2002) Geochemical monitoring of thermal waters in Slovenia: Relationships to seismic activity. Appl Radiat Isot 57:919–930. https://doi.org/10.1016/S0969-8043(02)00200-2

Figures

Figure 1

The study area (the Izmir fault zone (IF) is shown on the map with a red line; the Bornova fault are shown with yellow and blue lines)
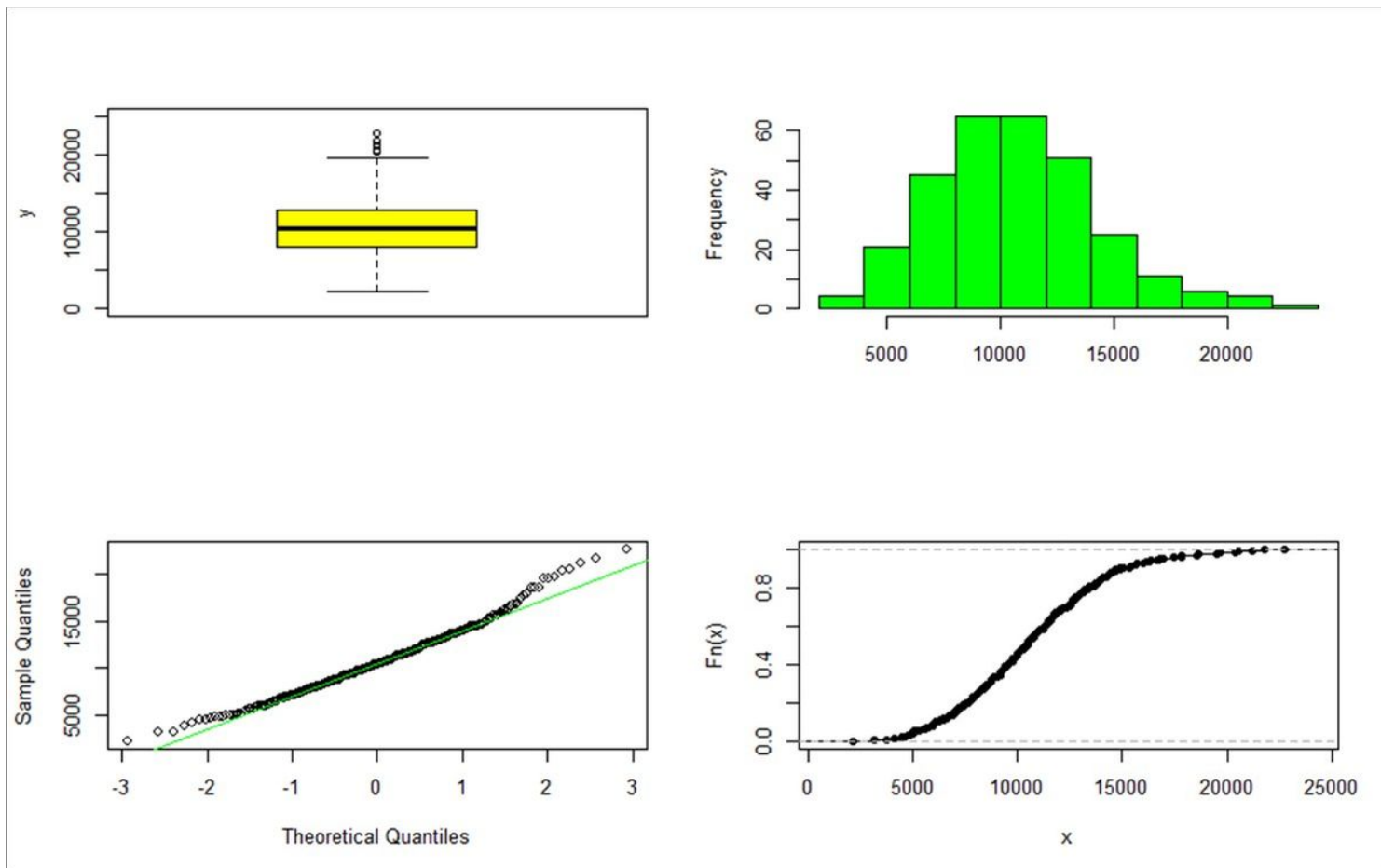
Figure 2

Boxplot, histogram, Q-Q plot, and ECDF plot of the activity of ^{222}Rn (Bq m^{-3}) in soil gas.
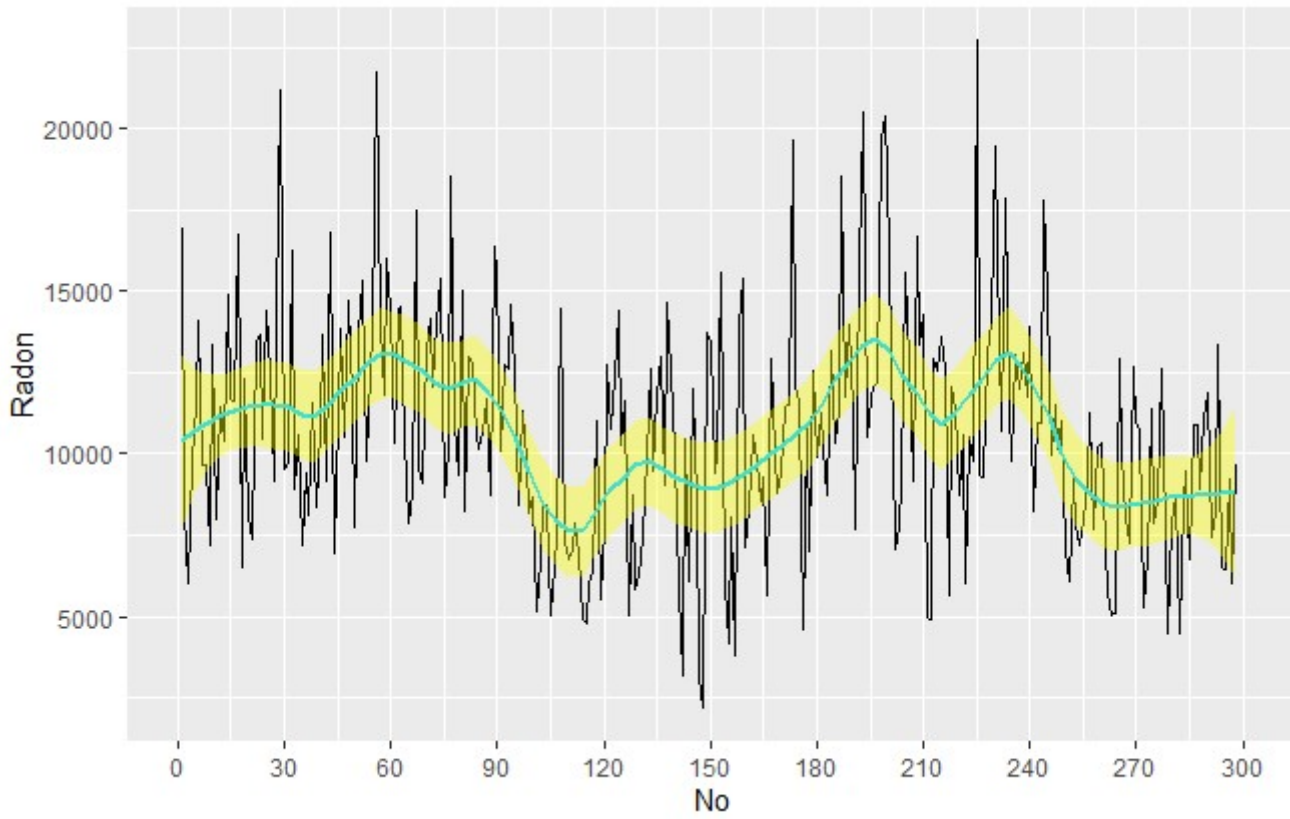
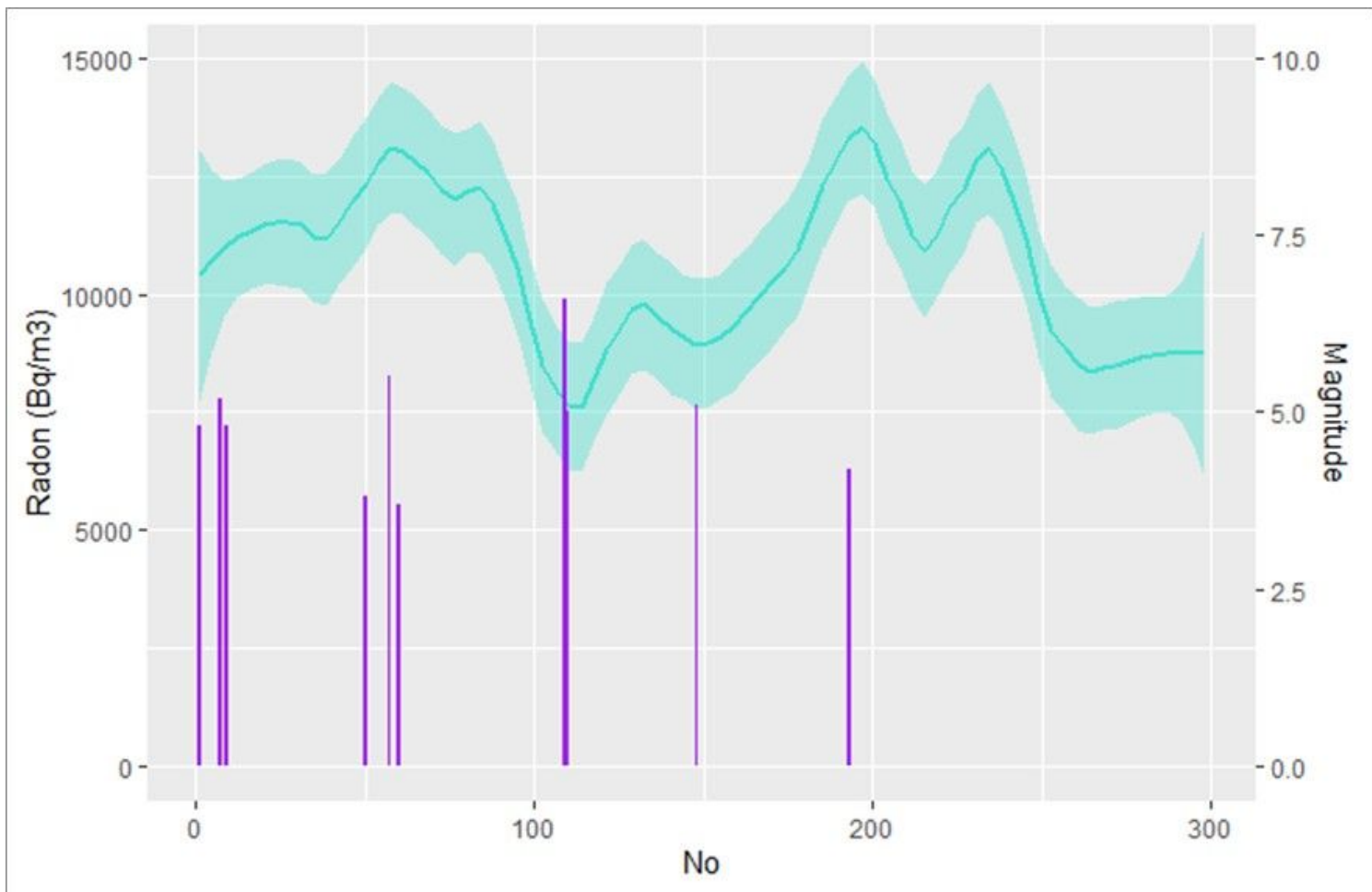**Figure 3**

Radon data (raw and trend line) during the study period

Figure 4

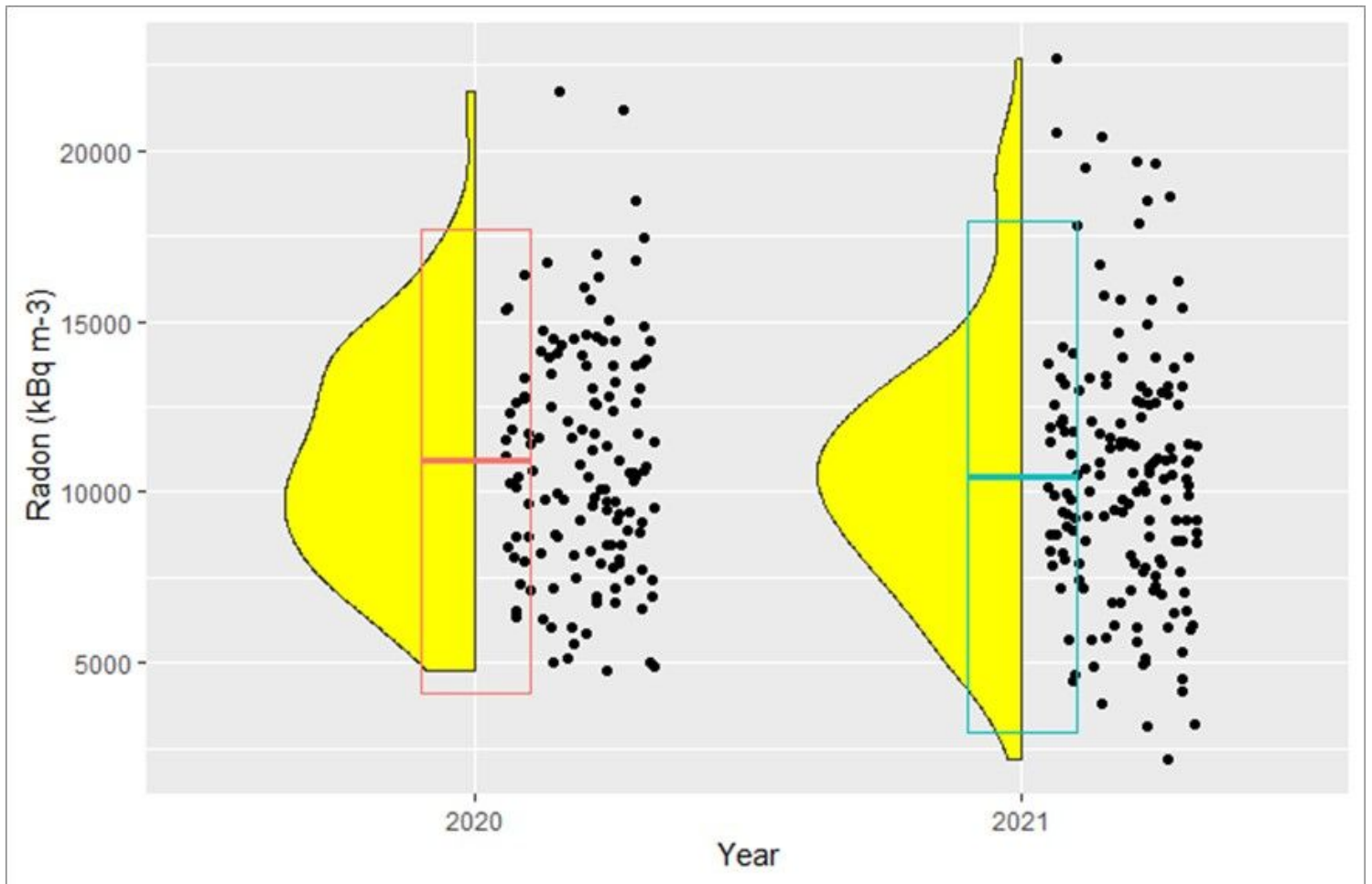The variation in radon (LOESS) and selected earthquakes

Figure 5

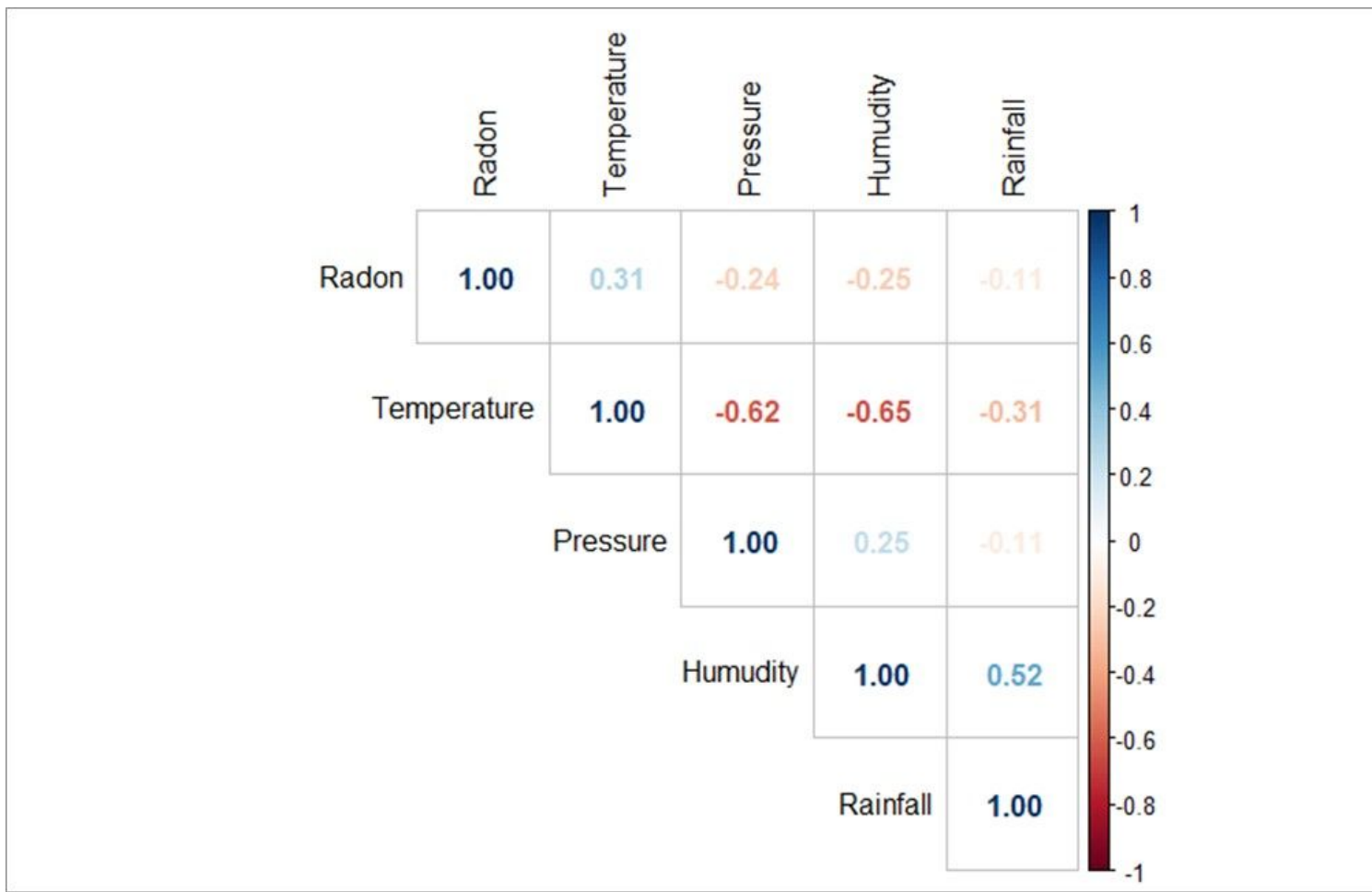The distribution of radon concentrations in consecutive years (2020 and 2021)

Figure 6

Correlogram of radon and meteorological parameters